MAPAN-Journal of Metrology Society of India (September 2022) 37(3):529–544
https://doi.org/10.1007/s12647-022-00575-0

ORIGINAL PAPER

Identification of Carbonaceous Species and FTIR Profiling of $PM_{2.5}$ Aerosols for Source Estimation in Old Delhi Region of India

S. Shankar[1], R. Gadi[1]*, S. K. Sharma[2] and T. K. Mandal[2]

[1]Indira Gandhi Delhi Technical University for Women, Delhi 110006, India

[2]CSIR-National Physical Laboratory, Dr. K. S. Krishnan Road, New Delhi 110012, India

Received: 09 December 2021 / Accepted: 27 May 2022 / Published online: 8 July 2022

Abstract: In this study, $PM_{2.5}$ samples from a traffic-influenced site in old Delhi were collected from January 2021 to June 2021 (January–March, 2021: months with regular activities; April–June, 2021: partially restricted months due to second wave of pandemic) and analysed to assess noteworthy effect on their infrared (IR) spectral features and carbonaceous content viz., organic carbon (OC) and elemental carbon (EC) and their sub-fractions with their link to major sources in the vicinity of the sampling site of Delhi. Absorbance peaks for the structural and functional groups for previously identified compounds associated with vehicular/combustion/biogenic emissions at the site were notable. Intensive peaks for C=C, C–H, O–H and NH_4NO_3 were observed on certain days pointing towards enhanced emission of the related compounds. Lower spectral peaks were observed for March and first half of April probably due to transitioning meteorological variables and imposed restrictions. Monthly variation in ratios, such as OC/EC, EC/TC and OM/OC, revealed about the probable emission sources. Comparatively higher peaks/values were observed during January, February and June. The overall results followed a general pattern of variation for regular days.

Keywords: ATR-FTIR; IR spectra; Organic carbon (OC); Elemental carbon (EC); $PM_{2.5}$

1. Introduction

Air pollution has become one of the global problems today, mainly, due to uncontrollable emissions of pollutants and their toxic effects on biotic and abiotic factors of the environment [1]. Once released into the atmosphere, the particulate matter (PM) is either fresh or undergoes aged deposition, traversion and secondary transformations which determine the residence time of the aerosols in atmosphere, thus affecting the ambient air quality [2–4]. Many studies have been conducted in recent past to trace impairing and lethal impacts of $PM_{2.5}$ and their organic constituents on fauna [5–9] as well as flora [10–12]. As a consequence, many upgraded fuels [13] and purification techniques for industrial emissions are being worked upon [14–16]. Organic constituents are considered as one of the most abundant components of urban PM2.5 (up to 90%). Total carbon consists of organic carbon (OC), elemental carbon (EC) and inorganic carbon (IC). OC contains light-reflective species, whereas, EC consists of light-absorbing species. IC is not considered at all in fine aerosol samples because it is mainly associated with coarse particulate matter (aerodynamic diameter, d_a between 2.5 μm and 10 μm) and is attributed to crust material [17]. EC (similar to black carbon) (which substantially absorbs tropospheric radiation, and cause visibility reduction), OC and sulphate aerosols do principally trigger climate change via radiative forcing since these can absorb as well as scatter radiations (both, solar and terrestrial) [18–21]. EC are generated predominantly by primary sources such as biomass burning/biogenic emissions and fossil fuel combustion, whereas, many anthropogenic and biogenic sources, along with secondary formations (mainly due to photo-oxidation) from precursor gases (e.g., toluene, isoprene) contribute to OC generation. Primary organic carbon (POC) and secondary organic carbon (SOC) constitute organic carbon in PM. Fossil fuel combustion and biomass burning act as direct emission source of POC in the ambient environment. Volatile organic species actively get oxidised in the atmosphere to SOC. The literature mentions to utilise thermo-optical analysis (TOA) for measuring OC, EC and

*Corresponding author, E-mail: ranugadi@igdtuw.ac.in

their fractional constituents in order to estimate secondary organic aerosol (SOA) formation [22, 23] thereby, apportioning definite sources at the site. Moreover, OC–EC subfractions and OC/EC ratios have been found to be associated with different sources of emissions and physicochemical atmospheric processes [22, 24, 25]. EC and OP (pyrolyzed carbon) can be detected by TOA due to their absorption tendency, unlike the light scattering property of OC [25]. Researchers have scarcely utilised Fourier transform infrared (FTIR) spectroscopy technique to obtain spectral signature of aerosol particles (both, PM_{10} and $PM_{2.5}$) for probable sources. This technique facilitates to efficiently examine the entire sample for distinct peaks of absorption related to definite chemical bonds and the functional groups, qualitatively. Attenuated Total Reflectance-Fourier Transform Infrared Spectrophotometer (ATR-FTIR) enables to examine the aerosol samples in their original state without prior preparation (extraction or derivatization). This method is non-destructive and rapid, and requires very small sample size ($\sim$ 2 mm^2) [26, 27]. The sample portion is rightly deposited on the ATR-crystal at which IR beam is incident at particular angle [27]. The quartz filters can be probed at absorption or transmission mode. In addition, the same filters can be examined for other characteristic features. This becomes advantageous in filter- and sampling- artefact reduction for studies. The light scattering by PM is inhibited by applying sample pressure tower (part of ATR accessory), thus eliminating the interferences; this can be achieved better in absorption mode of IR spectroscopy. Due to iteration of peaks at different wave numbers for same functional group and overlapped peaks for different functional groups at a single wavenumber, it is difficult to apply calibration method for quantification purposes [28]. However, some researchers [28–30] have tried to quantify broad functional groups, but no other way has been developed which could quantify each specific functional group with accuracy. Gilardoni et al. [31] measured and compared the OC and organic matter (OM) concentrations (at Chebogue Point, Nova Scotia, Canada, and Appledore Island, Maine, USA) obtained by TOA and FTIR; they observed that linearity of the correlations between OC and OM varied greatly. FTIR would be practically more elucidative for samples from areas having least probable sources of pollution. Studies are available for qualitative studies of functional groups present in aerosol samples [28, 29, 32–34]. As compared to conventional lower resolution analytical techniques, the penetration depth of IR beam is up to several microns [30], thus, suitable for studying PM collected on filters or in powdered form [26].

First half (i.e., January to March) of the study period signified unlock phase, whereas later half (i.e., April to June) signified partial lockdown due to re-emergence of COVID-19 (second wave) [35]. First half of the study period witnessed enhanced levels of $PM_{2.5}$, in Old Delhi region, as compared to usual trend as per the Continuous Ambient Air Quality Monitoring (CAAQM) data of Central Pollution Control Board (CPCB), India [36].

Delhi is listed among the world's top polluted cities. Since Old Delhi region has numerous sources of atmospheric pollutants [37, 38] and resources are available to sample and analyse atmospheric aerosols at the study area. Therefore, it has been attempted to identify contributions from probable sources of organic and inorganic functional groups present in collected $PM_{2.5}$ samples. Few studies have been reported in Delhi. Mishra et al. [39] and Goel et al. [40] performed qualitative and quantitative estimation of ambient $PM_{2.5}$ samples employing FTIR spectroscopic technique in New Delhi. However, no such studies have been reported in the Old Delhi region. The previous study in this region, undertaken by the same group has reported OC–EC content, its sub-fractions and related ratios in $PM_{2.5}$ [37]. Hence, it was intended to study the variations in spectral features, OC, EC, their sub-fractions and certain derived ratios keeping in view the different phases during the study period.

2. Methodology

2.1. Study Area

Delhi is the capital city with dense population ($\sim$ 16.8 million or 11,320 persons per square kilometre in 2011) and lakhs of manufacturing units spreading over $\sim$ 1483 km^2 as per the Census 2011 and *Economic Survey of Delhi*, 2018–19 [41]. Numerous manufacturing units of automobile parts are in the vicinity of the sampling site. $PM_{2.5}$ sampling was carried out at approximately 20 m height above the ground level at Indira Gandhi Delhi Technical University for Women (IGDTUW) Campus (28.66 N, 77.23 E) (Fig. 1) in Delhi, India. The campus is having Inter-State Bus Terminal (ISBT) in its close proximity (aerial distance $\sim$ 400 m) and is surrounded with busy highways, government offices and residential areas. Hence, traffic influence on the collected samples is highly expected at this site. Previous studies [42–47] have reported for various combustion sources of PM at this site.

2.2. Sampling of $PM_{2.5}$

Sampling of $PM_{2.5}$ ($d_a \leq 2.5$ µm) was conducted at IGDTUW Campus, Delhi by deploying fine particulate sampler (Model: Envirotech APM 550). Pre-combusted (at 550 °C) Quartz Fibre Filters (QFFs; 47 mm diameter) were utilised for $PM_{2.5}$ sampling and was carried out for 24 h

Set of original figures:

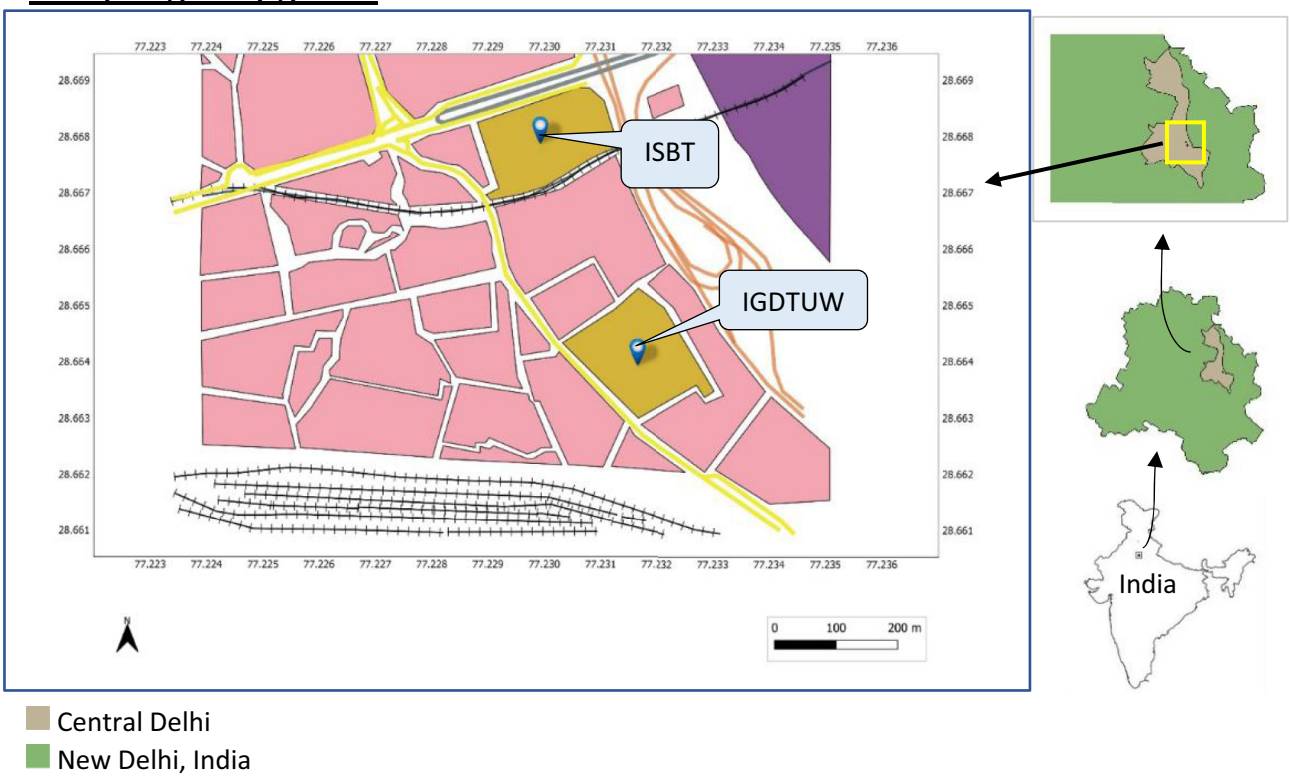

Fig. 1 Sampling site (IGDTUW) in Old Delhi region

(starting at 10:00 a.m.) twice a week from January–June, 2021. The filters (QFFs) were routinely desiccated for 24 h before and after sample loading, and stored at – 27 °C till analysis. The sampling protocol, data quality assurance, and control measures were adopted from the previous work [3, 4, 37, 38, 42–46]. Four representative samples in each month (n = 4) of the study period were selected for FTIR and OC–EC analyses.

2.3. Measurement

2.3.1. $PM_{2.5}$ and Meteorological Parameters

$PM_{2.5}$ mass (µg) was measured using gravimetric method. This was calculated by finding the difference between weight of loaded and unloaded QFFs. The obtained $PM_{2.5}$ mass (µg) was divided by the total volume of air passed while sampling in order to determine $PM_{2.5}$ concentration (µg m^{-3}).

Daily meteorological data were obtained from the CAAQM data repository of CPCB, India [36]. Meteorological data include temperature (°C), relative humidity (%), precipitation (mm) and wind speed (m/sec).

2.3.2. EC and OC

The OC and EC concentrations (sub-fractions of OC and EC) of $PM_{2.5}$ samples were examined by Thermal/Optical Carbon Analyzer (Model: DRI 2001A) on a $\sim$ 0.536 cm^2 filter punch from the loaded QFFs applying Interagency Monitoring of Protected Visual Environments (IMPROVE)-A protocol [37, 46]. The instrument operates by evolving carbon fractions and converting these to CO_2 (at each temperature step) under varying temperature and oxidation environments and further quantifying the liberated CH_4 using flame ionisation detector (FID). OC volatilizes to its sub-fractions at temperature ramps of 140 °C (OC1), 280 °C (OC2), 480 °C (OC3) and 580 °C (OC4) in pure helium atmosphere (non-oxidising). Combustion of EC takes place at 580 °C (EC1), 740 °C (EC2) and 840 °C (EC3) in helium (98%) and oxygen (2%) atmosphere. Instrument calibration is performed by analysing CO_2, balance helium gas and known amount of potassium hydrogen phthalate. The principle, calibration procedure and standard used are discussed in our previous publications [42–46]. To assess the OM content in the samples, the measured OC values were multiplied with a conversion factor of 1.8. This conversion factor is applicable to urban

areas considering extent of OM oxidation, formation of SOA and ageing of aerosols [46–48].

2.3.3. ATR-FTIR Analyses

In this study, qualitative analysis of functional groups and present bond information in the aerosol samples were taken using FTIR spectrometer (Model: SHIMADZU FTIR IRAffinity-1S). The instrument was operated using LabSolutionsIR software in order to visualise the spectra for each sample. An ATR (QUEST ATR) accessory (Diamond crystal) coupled with the equipment was utilised to acquire spectral data. A small circular fragment ($\sim$ 2 mm diameter) of the loaded sample was pressed onto the ATR crystal; hence, directly exposed to the IR radiation. Since, the samples were to be analysed for other chemical and physical parameters, IR spectra from a single location on the filters could be obtained. Same was applied to scan the blank filters and standard filters to acquire primary sources of information of spectral peaks of aerosol samples. The spectra of fine particulate matter were acquired within region of 3500–500 cm^{-1} with 4 cm^{-1} resolutions and 100 scans. Molecular vibrations and rotations caused due to IR absorption are uniquely attributed to structure and bond strength of each molecule. Also, absorption is proportional to concentration [49], therefore, spectra of unloaded filter were subtracted from the loaded one to plot final spectrum. An instrumental blank was scanned after every 8 sample scans. Ethanol was used to clean the ATR crystal and was let to dry-up completely before each scan to avoid any contamination. Skipping this step may reflect repeated peaks for -OH groups, and could mislead the results.

3. Results and Discussions

3.1. Variation in $PM_{2.5}$ and Meteorological Parameters

Figure 2 depicts trend of variation in $PM_{2.5}$ concentration and wind speed. $PM_{2.5}$ shows rise in concentration during January, April and June when the wind speed was lower. Similar trend was observed for February, March and May when $PM_{2.5}$ concentration was lower with higher wind speed. Figure 3 shows variation of Temperature (°C), Relative humidity (RH) (%) and Precipitation (mm) from January to June. Low temperature and high RH during January and February assisted in SOA formation. Figure 3 infers increased RH, lower wind speed and decreased temperature during January which is favourable condition for restricting PM movement. This could have led to aggravation of PM in January as represented in Fig. 2. However, during later period, i.e., after March, lower $PM_{2.5}$ levels might be due to effect of imposed restrictions.

The trends of variation in temperature and OC/EC ratio (Sect. 3.4) have been found quite similar. This indicates the impact of temperature on photo-chemical conversion of organic species in the atmosphere.

3.2. Variations in OC and EC

Figure 4a shows monthly average variation in OC and EC which exhibited decreasing trend from January to June ranging from 41.8 ± 18.3 to 9.8 ± 2.2 μg/m^3 for OC, and between 6.8 ± 8.4 and 2.7 ± 0.8 μg/m^3 for EC (± standard deviation). Despite decreasing trend from January to June, there was slight increase in OC and EC values during April which is similar to that observed by Gadi et al. [37]. No strange meteorological impact was observed during April; hence, it might occur due to emissions from anthropogenic sources. Since the sampling location is close to ISBT and highways, a significant contribution from vehicular emission is expected. In addition to meteorological impacts, there are other sources of direct emissions as well, such as biogenic sources of emission and residential wood combustion during winter. This gives rise in concentrations of POC [50, 51]. The variation of contribution of OC and EC in $PM_{2.5}$ followed an uneven trend throughout the duration; with a dip during February and slight increase during March.

In this study, anthropogenic emissions contributed, the most, to EC. EC is inert, thermally stable and possess resistance to atmospheric oxidation. This allows it to stay longer and be transported in the atmosphere. In comparison to OC, EC showed reduced monthly variation (Fig. 4a). However, it shows declining trend similar to OC. Since, EC acts as a marker for vehicular sources of emissions, lower values of it during April to June is justified due to restricted commercial activities after March due to re-emergence of COVID-19 pandemic. From Fig. 2, 4a, b, it is inferred that despite lower $PM_{2.5}$, OC and EC levels there is higher per cent composition of OC and EC in $PM_{2.5}$. However, 73.3 ± 4.4% of TC is attributed to OC, rest 26.7 ± 4.4% is contributed by EC (Fig. 4b) for which the obtained FTIR spectra of $PM_{2.5}$ samples (as discussed in next section) exhibited sharp peaks with intense absorption.

3.3. Variations in OC and EC Sub-fractions

Monthly variations in OC and EC sub-fractions have been presented in Fig. 5. Presence of volatile organic compounds (VOCs) is associated to significant OC1 (higher values during January: 12.2 ± 4.8 μg/m^3) and OC2 fractions (January: 7.2 ± 2.8 μg/m^3 and February: 7.7 ± 1.5 μg/m^3) and are likely to form secondary

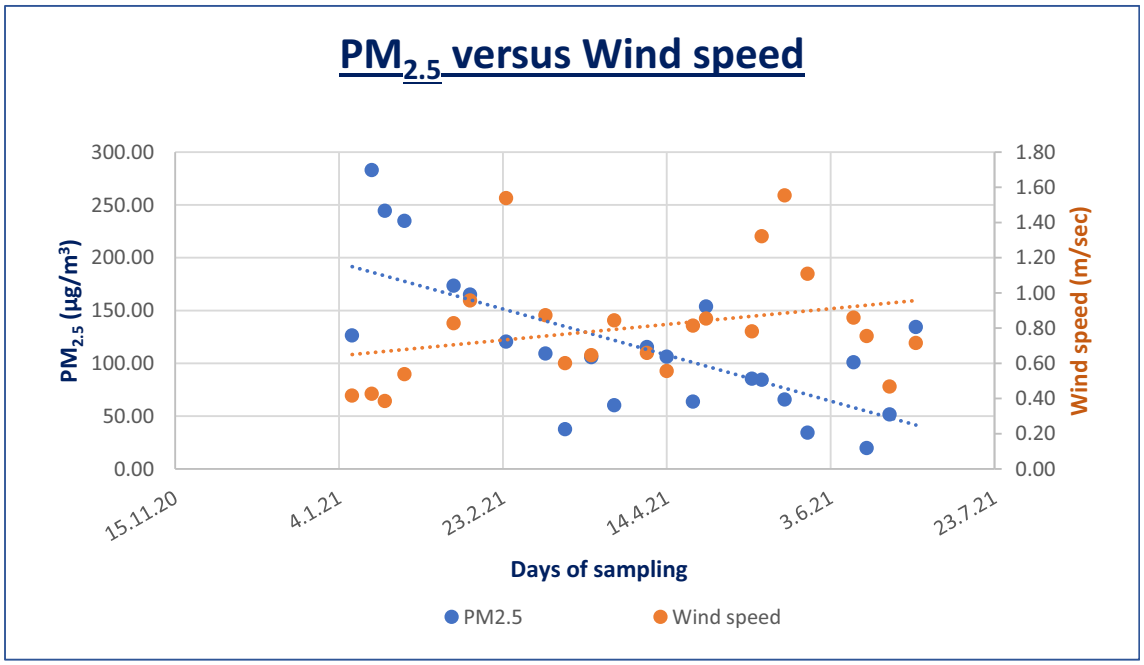

Fig. 2 Concentration of $PM_{2.5}$ and wind speed (WS) for the study period

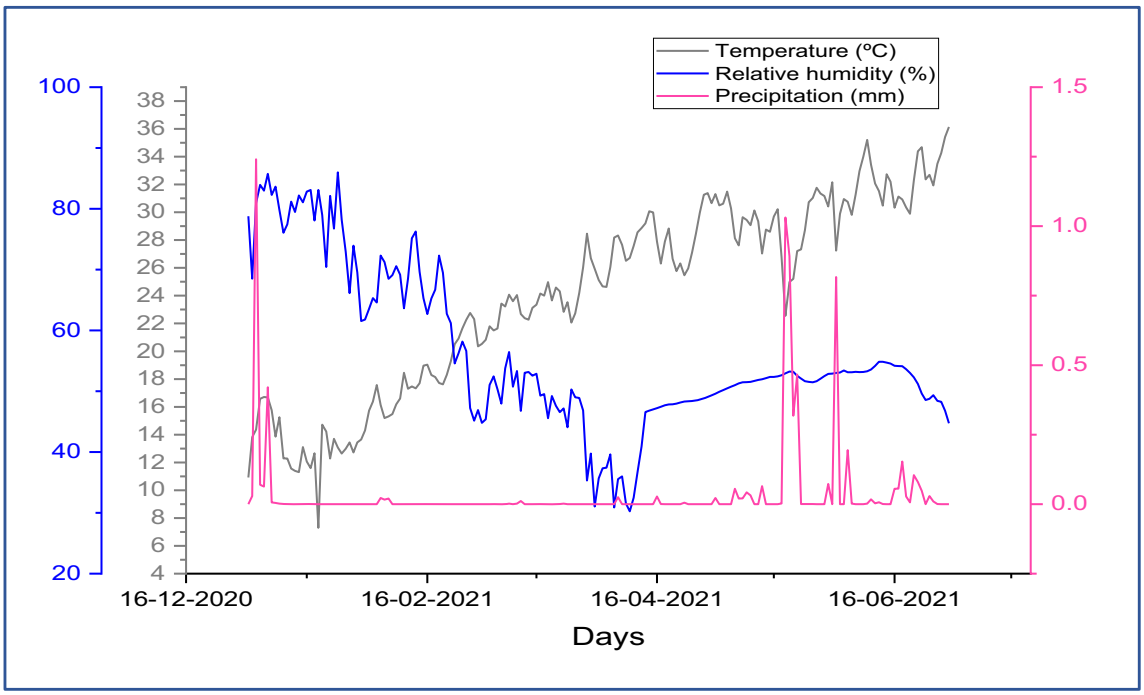

Fig. 3 Daily variation in temperature (°C), Relative humidity (%) and precipitation (mm) during the study period

products due to atmospheric conversion [52, 53]. Meanwhile, OC2 is also the representative of contribution from fossil fuel combustion and long-range biomass burning emissions which is in agreement with presence of SOC. Another important fraction, OP shows much higher values during January and February as compared to rest of the duration (averaging to 9.8 ± 2.6 µg/m^3), denoting incomplete combustion due to biomass burning and cooking. OC3 fraction indicates gasoline sources, nearby biomass burning and LPG exhaust (which is a common domestic source). Its contribution is surprisingly higher as compared to other OC fractions, during the imposed lockdown period

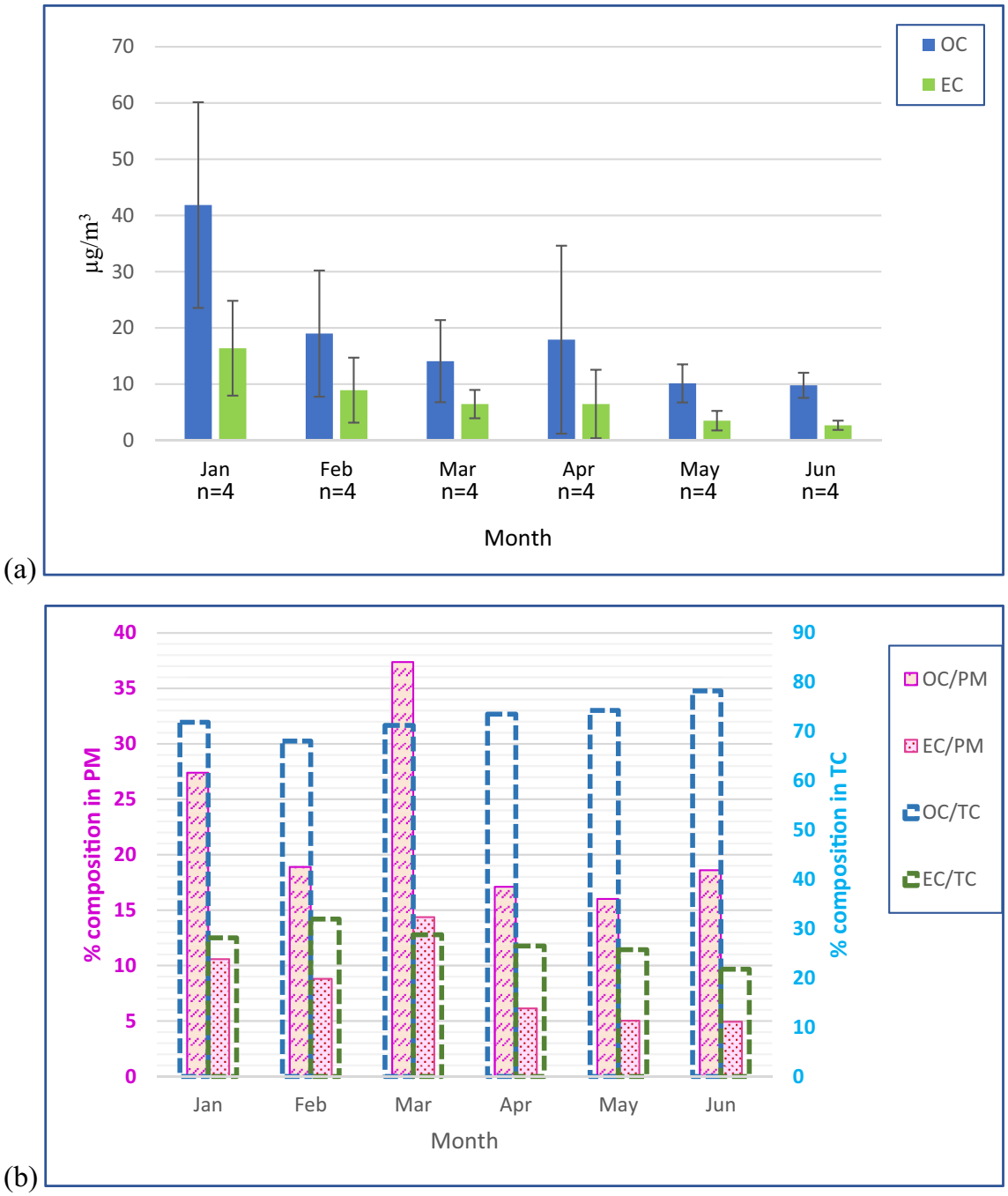

Fig. 4 Monthly average values for **a** OC and EC (µg/m^3) and **b** per cent contribution of OC and EC to total carbon (TC) and $PM_{2.5}$ for the study period

probably due to increased biomass burning and cooking emissions in the vicinity of the site. Presence of OC4 has been attributed to road dust [46, 53] which has been reflected in the FTIR results (as explained in Sect. 3.7). This may be the reason for OC4 being the least varying OC-fraction among all the four fractions (OC1–OC4).

Low EC fractional abundance, as compared to OC fractions, especially EC2, indicates for reduced contributions from coking related factories/plants [24, 53].

Local biomass burning emission is also attributed to *char EC* (cEC = EC1 − OP) [20, 23] and soot EC (sEC = EC2 + EC3) is indicative of diesel emissions. During normal days, there were many nearby sources such as street-food vendors and sidewalk dwellers, which may

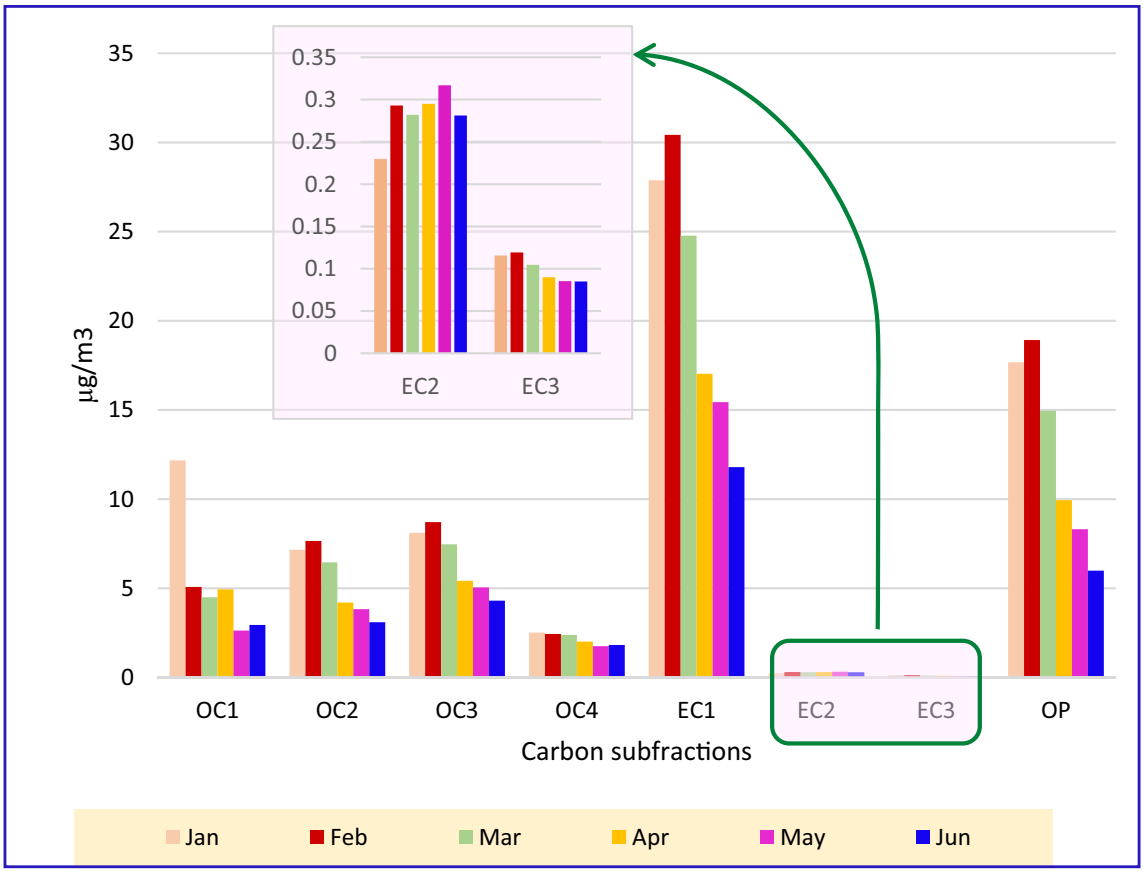

Fig. 5 Monthly variation in mass concentration (µg/m^3) of carbon sub-fractions (OC1, OC2, OC3, OC4, EC1, EC2, EC3 and OP) for the studied duration

contribute to cEC during January to March. As presented in Fig. 6, char-EC correlated strongly (R^2 = 0.94) with total EC unlike soot-EC (R^2 = 0.12). This indicated for biogenic emissions as the major contributor in EC-fraction [46, 51, 54].

3.4. Variation in OC/EC and EC/TC Ratios

The trend of variations for OC/EC ratio and temperature were quite similar. This indicated the impact of temperature on photo-chemical conversion of organic species in the atmosphere. The OC/EC ratio would be higher if the average OC concentration is higher; it seems to be associated with their regional or long-range transport. The significant linear correlation (R^2 = 0.94) between OC and EC indicates similar sources of emissions. The Q–Q plot for OC and EC showed that the sample data were not normally distributed. The points showed the deviation of the data from the straight fitted line (Fig. 7a, b). However, these plots followed similar pattern indicating their higher correlation. Earlier, Gadi et al. [37] had observed high correlation with R^2 = 0.83 (Fig. 7c) at the selected site. As discussed in Sect. 3.2, OC and EC showed declining trend throughout the studied duration, but the monthly average of OC/EC ratios ranged between 2.2 ± 0.2 to 3.8 ± 0.4 (Fig. 8). This indicates that the ratio in June tended to reach beyond 4 which represents contribution from wood and coal combustion [55, 56]. Arithmetically, this may also be attributed to more decrease in EC concentrations as compared to OC concentrations. Furthermore, this might be due to regional influence of SOC generated by agricultural burning. The values of OC/EC ratio between 1.5 and 4 is indicative of gasoline-driven vehicles [55, 56]. During May and June, the biomass is used by local residents for cooking purposes only and not for residential heating, hence, there might be influence of traffic and biogenic emissions. This has also been indicated by slight increase in EC/TC ratio (Fig. 8) during May & June (May > June) indicating diesel emissions [30]. This was probably due to increase in transportation and commercial activities due to plying of vehicles and medical exigency and other emergency services during that duration. Trend of increase in EC/TC value was observed from January to June ranging between 0.28 and 0.32, which increased with increase in fresh emissions [52, 60]. This infers more SOA contributions during unlock phase.

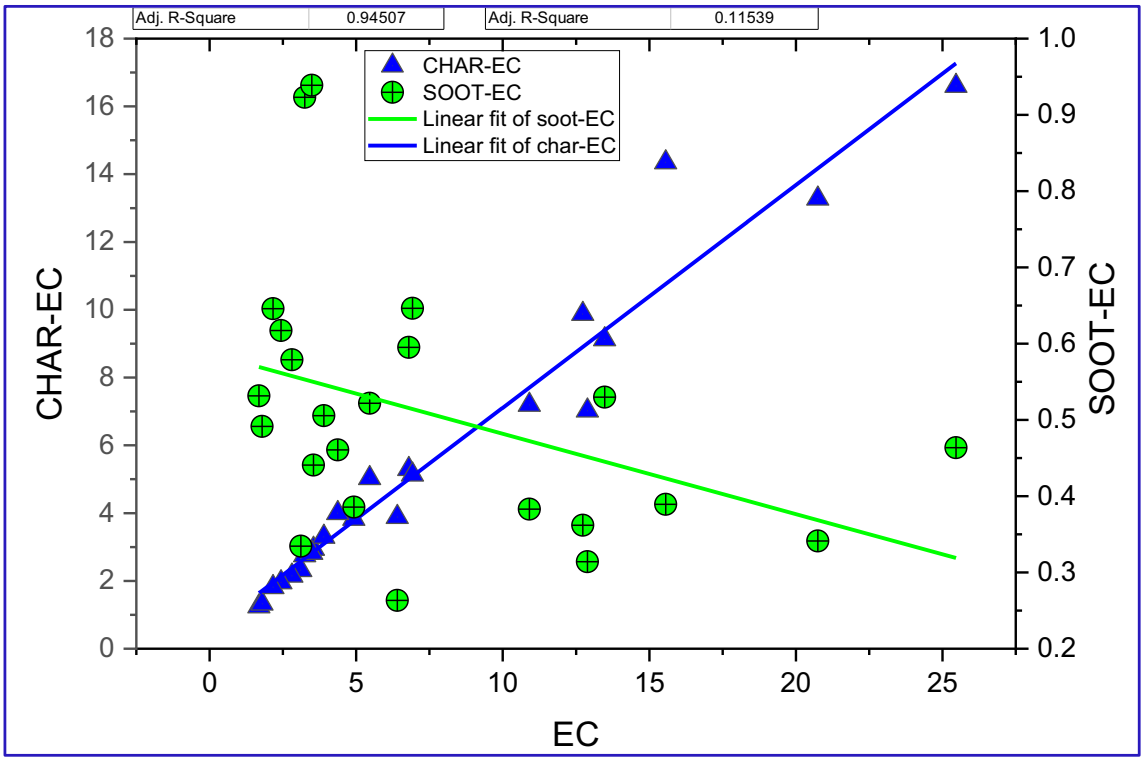

Fig. 6 Correlations between EC (μg/m^3) and char-EC (blue), and EC and soot-EC (green) for the study period

3.5. Estimation of Primary Organic Carbon (POC) and Secondary Organic Carbon (SOC)

In order to understand the contributions from primary sources or secondary formation of organic aerosols, the widely used EC tracer method has been applied here. The POC and SOC concentrations were estimated using the formula [48], where $(OC/EC)_{min}$ is the minimum value of OC/EC ratio in the sample dataset:

$$POC = EC * (OC/EC)_{min} \quad (1)$$

$$SOC = OC - POC \quad (2)$$

Figure 9 shows a declining trend of monthly values for POC and SOC estimation ranging from 32.1 ± 12.7 to 14.0 ± 3.2 and from 11.9 ± 4.6 to 1.3 ± 1.0, respectively, for the studied duration. Since, it is the harvesting time for winter crops in the adjacent region of the sampling area, stubble-burning may influence the SOC values during June. SOC also indicates the longer atmospheric residence of biogenic—(e.g., isoprenes, terpenes) and petrogenic-VOCs (e.g., aromatics, aliphatics, carbonyls) [57]. This may be correlated with comparatively higher SOC levels during period of unlock. Higher values for POC during January and February, in comparison to SOC, reflects comparatively more fresh contributions to ambient aerosols. As observed, both the variables showed gradual decrease till June.

3.6. Estimation of OM/OC Ratio

Xing et al. [58], in their study designated an OM/OC ratio of 1.4–1.6 for urban areas and 2.1 for rural sites. In this study, January depicted much higher OM/OC ratio (4.0 ± 1.7) than rest of the months as shown in Fig. 9. This may be correlated with biogenic emissions due to residential heating and favourable meteorological conditions, for less traversion of pollutants, during January. It can be high due to high sugar content and carboxylic acid content [59] as reflected in the IR spectra of active period (Sect. 3.7; Fig. 10). The OM/OC ratio also depends upon the volatility and gas-particle partitioning, thereby, ageing of the aerosol [60]. Therefore, the SOC and OM/OC ratio obtained for partial lockdown duration indicates the contribution of secondary and aged particulate matter in the ambient air at the sampling site.

3.7. ATR-FTIR Analysis of $PM_{2.5}$

As per the qualitative analysis of ambient $PM_{2.5}$ almost similar peaks were observed in all samples from January to June (2021) suggesting similarity in structural and functional groups. However, the peak intensity varied as a function of meteorological variables and prevailing/absent sources. The identified functional groups and bonds (absorption spectra) as function of wave numbers have been

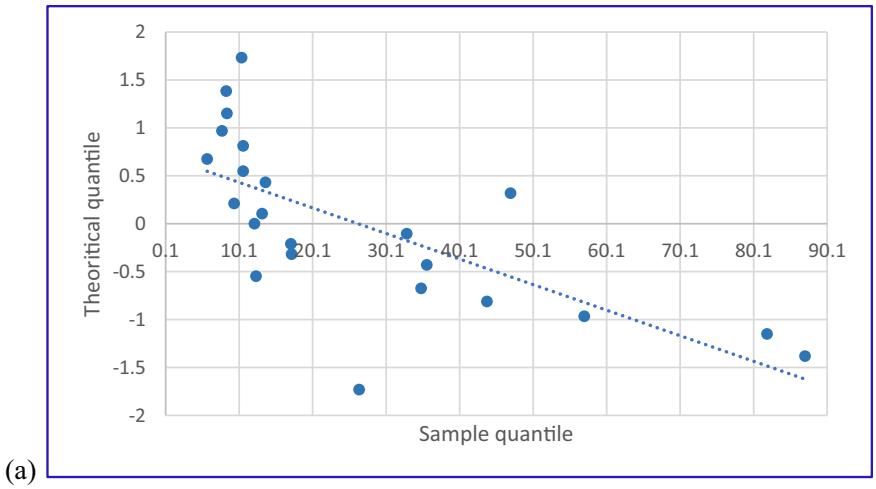

(a)

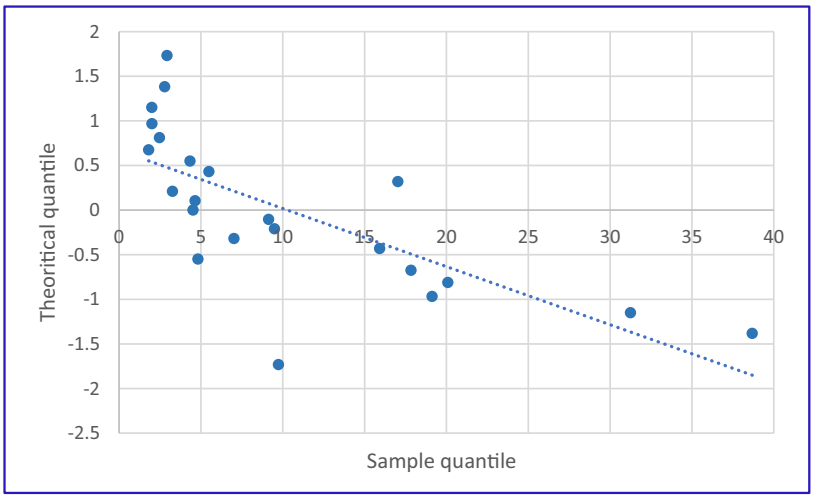

(b)

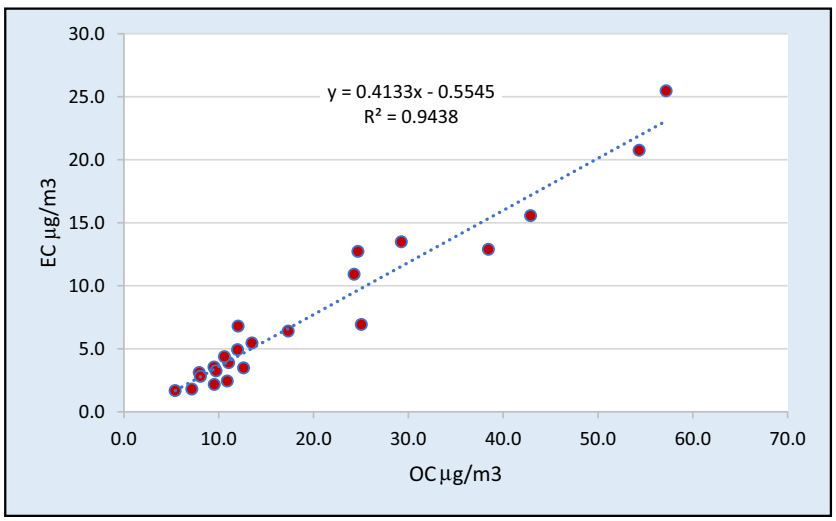

(c)

Fig. 7 Q–Q plots of **a** OC, **b** EC; and **c** correlation between OC & EC in the $PM_{2.5}$ samples for the study period

listed in Table 1. Absorbance analyses of samples show that they can be classified according to band similarity. The absorbance spectra of ambient aerosols demonstrate the functionalities which belong to major classes of organic/inorganic compounds and are attributable to definite emission sources. It is well established that the abundance

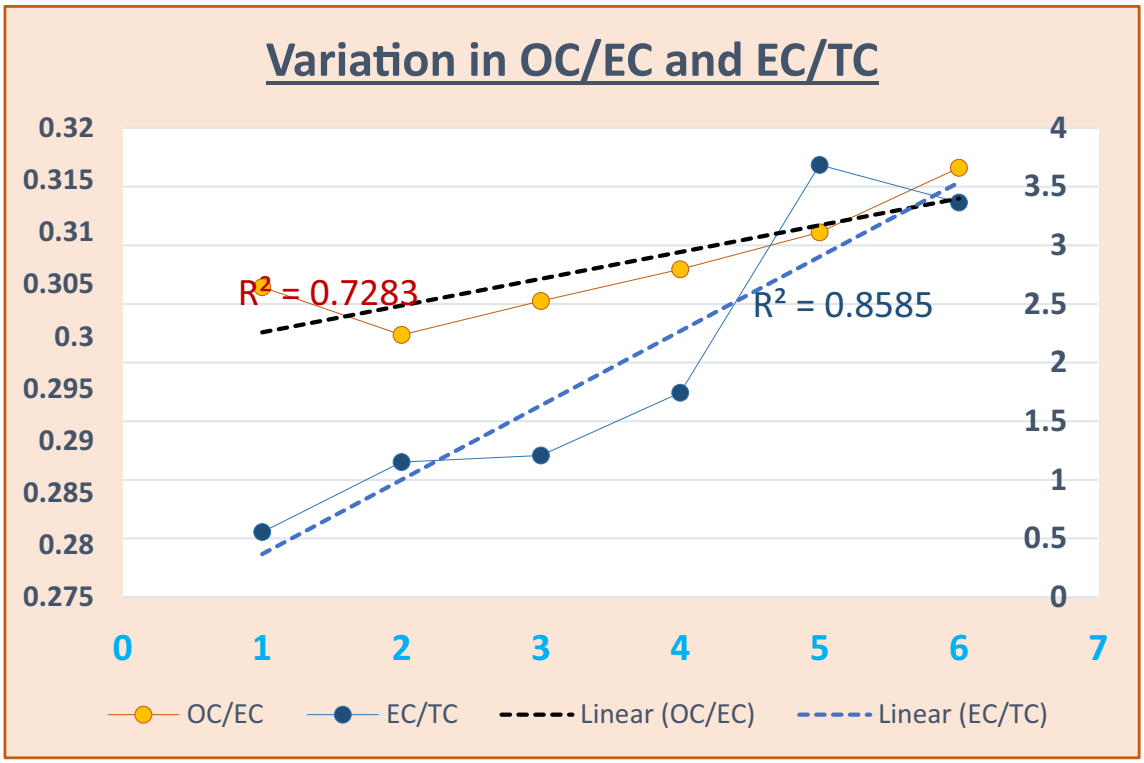

Fig. 8 Monthly average variation in OC/EC and EC/TC ratio for the study period (*1–6: January to June*)

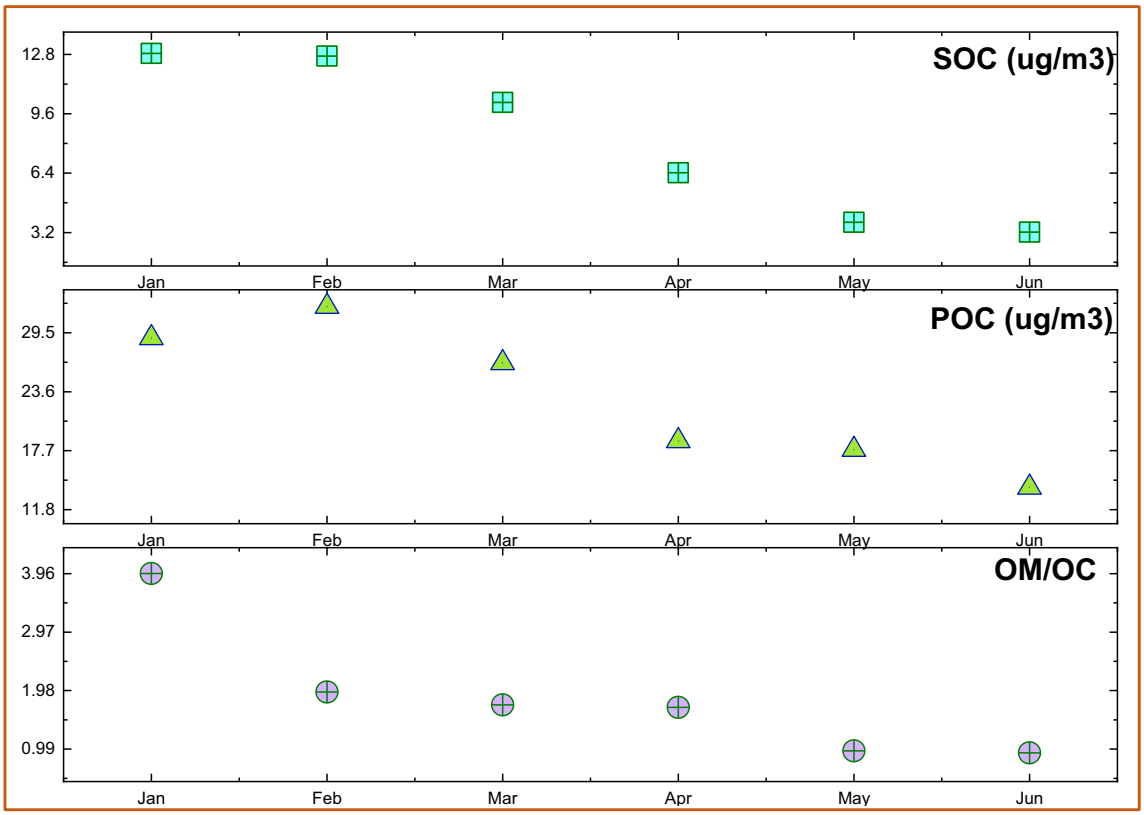

Fig. 9 Monthly variation in SOC, POC and OM/OC ratio for the study period

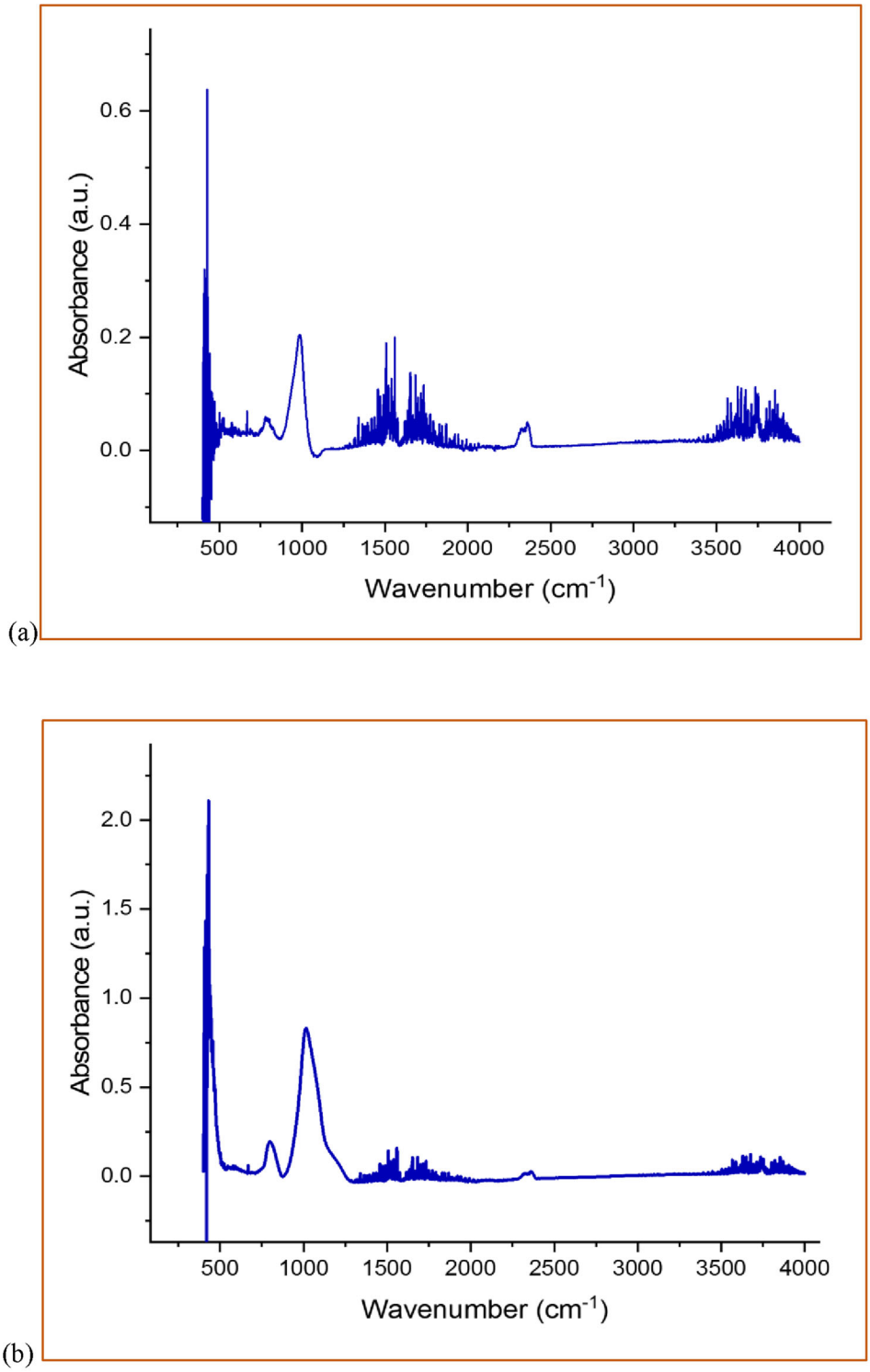

Fig. 10 Representative FTIR spectra of $PM_{2.5}$ samples during **a** normal and **b** partial lockdown days at sampling site in Old Delhi region for the studied duration

of chemical functionalities depends upon the emission-source properties as well as meteorological factors. Figure 10a, b shows the representative FTIR spectra of $PM_{2.5}$ samples during unlock and partial lockdown days, respectively. Absorbance between ~ 3600 and 3700 cm^{-1} represent dust and minerals present in the PM samples [24, 47, 53]. However, it has not been emphasised in this study because no major dust-events were observed around the sampling site. 3130–3550 cm^{-1} range is an intensive feature of O–H stretch in alcohols/phenols and acids. In addition to O–H stretching, the spectra within 2600–3000 cm^{-1} indicate absorption by saturated C–H

Table 1 Peaks of functional and structural groups identified in $PM_{2.5}$ samples for January–June, 2021

S. no.	Wavenumber (1/cm)	Identified groups	References
1.	3600–3700 cm^{-1}	Dust and minerals	[24, 47, 53]
2.	3310–3320 cm^{-1}	Alkyne C–H stretch	[31, 63]
3.	3130–3550 cm^{-1}	O–H from alcohols & polysaccharides	[31]
4.	3000 cm^{-1} and 3150 cm^{-1}	C=C–H from unsaturated chains and aromatic rings	[62]
5.	2600–3000 cm^{-1}	Saturated C–H	[31]
6.	2960 cm^{-1}	Asymmetric stretching of aliphatic CH_2	[26]
7.	2916 cm^{-1}	Aromatic C–C–H	[28, 33]
8.	2852–2922 cm^{-1}	Aliphatic C–C–H stretches	[28]
9.	2850 cm^{-1}	Aliphatic CH stretch	[26]
10.	2100–2260 cm^{-1}	Acetylene C≡C bonds	[63]
11.	1735 cm^{-1}	Ester and carbonyl	[26]
12.	1735 cm^{-1}	Acid carbonyl C=O	[31, 50]
13.	1716 cm^{-1}	Non-acid carbonyl C=O	[33]
14.	1700 cm^{-1} and 1770 cm^{-1}	Corresponds to vibration of carbonyl groups of carboxylic acids	[63]
15.	1705 cm^{-1}	Aldehydic and ketonic carbonyl C=O	[32]
16.	1654 cm^{-1}	Carboxyl C=O	[50, 63]
17.	1650–1690 cm^{-1}	Amide	[33]
18.	1630 cm^{-1}	Aromatic amides and organic amine and nitrate	[2]
19.	1606 cm^{-1}	Aromatic C=C	[28]
20.	1596 cm^{-1}	Aromatic C=C	[33]
21.	1580–1650 cm^{-1}	NH_2 group of amino acids or amines	[26]
22.	1530–1600 cm^{-1}	C–C inter-ring stretches of nitro-PAHs	[26]
23.	1521–1591 cm^{-1}	Nitro-group asymmetric stretching	[26]
24.	1508 cm^{-1}	Aromatic nitro group	[26]
25.	1450 $cm^{-1,}$	Aliphatic C–C–H	[26]
26.	1435 cm^{-1}	Aromatic C–C–H	[28, 33]
27.	1410–1440 cm^{-1} and 3020–3048 cm^{-1}	Ammonium ions	[34]
28.	1350 cm^{-1}	Nitro-group symmetric stretching	[26, 27]
29.	1335–1410 cm^{-1}	Nitrate ions	[28]
30.	1300 cm^{-1}	C–N stretches	[26, 70]
31.	1300 cm^{-1}—1500 cm^{-1}	Biomass burning emission	[65]
32.	1280 cm^{-1}	Organonitrates	[65, 66]
33.	1100 cm^{-1} and 600 cm^{-1}	Sulphate ions	[27]
34.	1087 cm^{-1}	Asymmetric stretching vibration of sulphate ions	[45, 66]
35.	1000 cm^{-1}	Asymmetric stretching vibration of O–Si–O	[49]
36.	800 cm^{-1}	bending vibration of O–Si–O	[66]
37.	780 cm^{-1}	C–H out-of-plane bends	[33]
38.	610–680 cm^{-1}	Alkyne C–H stretch	[63]
39.	500–670 cm^{-1}	Black carbon	[70]
40.	400–500 cm^{-1}	Brown carbon	[70]

stretch [28]. O–H stretch vibrations in this region are mainly due to alcohols and sugars originating from biogenic sources and biomass burning emissions and shows wide shoulder at 3400 cm^{-1} [27, 29]. Band structures between 3000 and 3150 cm^{-1} are good indicators of unsaturated (C=C–H) and aromatic rings in the sample [61]. Both symmetric and asymmetric stretching of CH_2 (aliphatic) groups are responsible for peak at 2960 cm^{-1} in few samples, whereas aliphatic C–C–H group shows peak at 1450 cm^{-1}. Sharp absorbance peaks observed at 2850 cm^{-1} are indicative of aliphatic C–H stretching vibration from ambient aerosols [31]. The absorbance peaks between 2000 and 2750 cm^{-1} have not been identified in most of the reported literature; however, a study

[62] has revealed that the very uncommon acetylene (C ≡ C) bonds are identified within 2100–2260 cm^{-1} range which can be di-/mono-substituted. Similar weak peaks of absorbance for alkyne C–H stretch and bends should be present within 3310–3320 cm^{-1} and 610–680 cm^{-1}, respectively.

Presence of aromatic C=C and strong aliphatic C–C–H stretches due to traffic emissions (typically, diesel/gasoline) are confirmed due to peaks at 1596 cm^{-1} [30] and between 2852–2922 cm^{-1} range [29], respectively. Absorbance for carboxyl and carbonyl C=O group are reflected at 1654 cm^{-1} and 1700 cm^{-1}, respectively. A sharp absorption band for carbonyl indicates for SOA formation. Acid and non-acid carbonyl (C=O) absorbance (1716 cm^{-1} and 1735 cm^{-1}) [29, 30] were highlighted during summer time, particularly during May and June. This points towards photo-chemical oxidation and secondary organic aerosol formation. In contrast to summer days the spectra for winter time demonstrate significantly different patterns of aromatic C=C (1606 cm^{-1}) and C–C–H groups (1435 cm^{-1} and 2916 cm^{-1}). During high biomass burning emission period, band at 1745 cm^{-1} appeared to be prominent and wider compared to rest of non-emission days, indicating occurrence of photo-chemical oxidation and atmospheric transportation.

Shape and shoulders of the peaks indicate the presence of overlapping absorption of different types of functional groups and/or bonds. At around 1735 cm^{-1}, IR is absorbed by esters and carbonyl groups. Aromatic and aliphatic carboxylic acids should be present in ambient PM and esters are less likely components (if it is not a wide peak). Aromatic amides and organic amines and nitrates have shown absorption shoulder at 1630 cm^{-1}. An absorption in N–H and $–NO_2$ groups are majorly attributed to light absorbing brown carbon [30]. Shoulder absorbance peaks between 1700 and 1770 cm^{-1} corresponds to vibration of carbonyl groups of carboxylic acids, which are generated by photo-oxidation of combustion products [62]. Absorbance at 1705 cm^{-1} is due to aldehydic and ketonic carbonyl C=O group. Numerous carbonyl and amide groups in the samples indicate presence of anhydro-sugars (for instance, levoglucosan), a major trace/indicator for biomass burning emission. Sharp intense peaks in May and June samples as compared to rest of the study period, ranged within 1530–1600 cm^{-1} attributed to C–C interring stretches of nitro-PAHs and other aromatic rings [31, 62, 63].

According to the study [31] of nitrated-polyaromatic hydrocarbons (n-PAHs), the nitro-group showed symmetric and asymmetric stretching vibrations at 1350 cm^{-1} and 1521–1591 cm^{-1} range, respectively. The peaks from samples of January, February and March were slightly wide but prominent at 1379 cm^{-1}, 1432 cm^{-1} and 1630 cm^{-1}. Absorbance at 1379 cm^{-1} was shown during later half of April, only NH_4NO_3/C-O or polysaccharides and aliphatic/aromatic carbon (1300–1500 cm^{-1}) showed traces of biomass burning emission, which were negligible in May [65]. It may be correlated to slight increase in level of OC1 (which is clear indicator of biomass emission) and EC2 (indicator of coal combustion and vehicular emission) during April (discussed in Sect. 3.3). The spectral results (mostly between 1330–1575 cm^{-1}, 1625–1860 cm^{-1} and ~ 3400 cm^{-1}) for June are in agreement with that of OC–EC results, both indicative of SOC and long-range transport of biogenic tracers. It is probably because of stubble burning emissions in harvesting month (June) in North India. Polidori et al. [31] reported the presence of ammonium nitrate in their samples which could mask the absorbance due to organic functional groups. Absorbance at 1508 cm^{-1} contributes to identification of aromatic nitro group. The sample scans reflected the presence of absorbance within range of 1335–1410 cm^{-1} (nitrate ions) and 1410–1440 cm^{-1} and 3020–3048 cm^{-1} (ammonium ions) [23, 25, 58, 65]. The peaks between 1270 and 1650 cm^{-1} are indicative of presence of ions such as nitrate and ammonium ions, C=C bonds (aliphatic/aromatic), and aliphatic CH_3, aromatic nitro, C–N, C–O and OH functional groups. Greater absorbance in this region in February signifies for biogenic emissions from the nearby region. A broad absorbance in 1580–1650 cm^{-1} range denotes amine (NH_2) group of amino acids or amines. Absorbance due to C–N bond of nitro-group (in all samples, except May) and C–H (out-of-plane) vibrations are reflected at 1300 cm^{-1} and 780 cm^{-1}, respectively, in all samples which might be due to more diesel emissions (nitro-PAHs) and other sources [31]. No clear peak was observed at ~ 745 cm^{-1} for skeletal vibrations of C–C stretch as reported by Polidori et al. [31] which might have occurred due to solvent constituents. The presence of carbonyls (C=O), saturated and unsaturated C–H and O–H functionalities is associated with the presence of SOA in $PM_{2.5}$ samples [29]. As per the results obtained from OC, EC and their sub-fractions, there is high indication of contributions from vehicular and biogenic emissions in the obtained functional groups and chemical bonds. Sulphate ions should be present in atmosphere as a result of primary and secondary formations and their peaks should be present at 1100 cm^{-1} and 600 cm^{-1} in all the samples. A shoulder peak at 1087 cm^{-1} can be observed due to asymmetric stretching vibration of sulphate ions. Asymmetric stretching vibration of O–Si–O have been found to show the peak at around 1000 cm^{-1} [48] and at 800 cm^{-1} due to bending vibration [66], both of which are present in SiO_4^{4-}. Studies related to dust events, especially in coarse dust, have found a weak peak at ~ 1010 cm^{-1} and 914 cm^{-1} attributed to Al–(OH) [67]. Al–(OH) confirms the presence of kaolinite peak

which is absent in this study, since there are no such sources [68, 69]. High absorption peaks for black and brown carbon can be observed at 400–500 cm^{-1} and 500–670 cm^{-1} [70].

4. Conclusion

In this study, it has been attempted to identify contributions from probable sources of organic and inorganic functional groups present in $PM_{2.5}$ samples. It was also intended to correlate the variations in peaks on the basis of OC–EC analytical data from January to June, 2021. Variability in spectral features, OC, EC, their fractions and certain derived ratios have also been estimated keeping in the view the partial lockdown phase during the study period.

Following observations were inferred by computing different ratios derived from OC and EC concentrations and correlating with the obtained IR-peaks: OC and EC values showed positive correlations, indicating similar sources. However, meteorological impacts cannot be denied. IR peaks were intense in January and June, possibly due to enhanced traffic emissions and other burning/combustion sources. Functional markers such as aromatic C=C and aliphatic C–C–H bonds/groups indicated presence of traffic emissions (diesel/gasoline) in all months, but reduced effect in February and May was probably due to favourable meteorological conditions and comparatively lesser emissions, respectively. This is in accordance with $PM_{2.5}$ concentration. Functional groups and bonds spectra for samples from the restricted period were consistent with that of source analysis for OC–EC and their sub-fractions.

References

1. A. Sen, A.Y. Nazeer Ahammed, B.C. Arya, Tirthankar Banerjee, G. Reshma Begam, B.P. Baruah, A. Chatterjee, A. K. Choudhuri, A. Dhir, T. Das, P.P. Dhyani, Atmospheric fine and coarse mode aerosols at different environments of India and the Bay of Bengal during winter-2014: implications of a coordinated campaign. MAPAN-J. Metrol. Soc India, **29**(4) (2014) 273–284
2. O. Sevenou, S.E. Hill, I.A. Farhat and J.R. Mitchell, Organisation of the external region of the starch granule as determined by infrared spectroscopy. Int. J. Biol. Macromol., *31* (2002) 79–85.
3. D. P. Singh, R. Gadi, T. K. Mandal, C. K. Dixit, K. Singh, T. Saud, N. Singh, P. K. Gupta, Study of temporal variation in ambient air quality during Diwali festival in India. Environ. Monit. Assess., **169**(1–13) (2010).
4. D.P. Singh, R. Gadi and T.K. Mandal, Emissions of polycyclic aromatic hydrocarbons in the atmosphere: An Indian perspective. Hum. Ecol. Risk Assess., *16* (2010) 1145–1168.
5. N. Künzli, R. Kaiser, S. Medina, M. Studnicka, O. Chanel, P. Filliger, M. Herry, F. Horak Jr., V. Puybonnieux-Texier, P. Quénel, J. Schneider and H. Sommer, Public-health impact of outdoor and traffic-related air pollution: a European assessment. Lancet, *356* (2000) 795–801.
6. M. Kampa and E. Castanas, Human health effects of air pollution. Environmental pollution, *151* (2008) 362–367.
7. K. Naddafi, M.S. Hassanvand, M. Yunesian, F. Momeniha, R. Nabizadeh, S. Faridi and A. Gholampour, Health impact assessment of air pollution in megacity of Tehran, Iran. J. environ. health sci., *9* (2012) 1–7.
8. R.J. Sram, B. Binkova, M. Dostal, M. Merkerova-Dostalova, H. Libalova, A. Milcova, P. Rossner Jr., A. Rossnerova, J. Schmuczerova, V. Svecova, J. Topinka and H. Votavova, Health impact of air pollution to children. Int. J. Hyg. Environ. Health, *216* (2013) 533–540.
9. Y. Raziani and S. Raziani, The Effect of Air Pollution on Myocardial Infarction. Chem. Rev., *3* (2021) 83–96.
10. C. Ramos de Rainho, S. Machado Corrêa, J. Luiz Mazzei, C. Alessandra Fortes Aiub, I. Felzenszwalb, Genotoxicity of polycyclic aromatic hydrocarbons and nitro-derived in respirable airborne particulate matter collected from urban areas of Rio de Janeiro (Brazil), Biomed Res. Int. (2013).
11. P.K. Rai, Impacts of particulate matter pollution on plants: Implications for environmental biomonitoring. Ecotoxicol. Environ. Saf., *129* (2016) 120–136.
12. D. Karmakar, K. Deb and P.K. Padhy, Ecophysiological responses of tree species due to air pollution for biomonitoring of environmental health in urban area. Urban Clim., *35* (2021) 100741.
13. EPA, 2016; (https://www.epa.gov/sites/production/files/2016-07/documents/select-ghg-results-table-v1.pdf)
14. C. Posten and G. Schaub, Microalgae and terrestrial biomass as source for fuels—a process view. J. Biotechnol., *142* (2009) 64–69.
15. S. Hansen, A. Mirkouei and L.A. Diaz, A comprehensive state-of-technology review for upgrading bio-oil to renewable or blended hydrocarbon fuels. Renew. Sustain. Energy Rev., *118* (2020) 109548.
16. A. Keskin, M. Şen and A.O. Emiroğlu, Experimental studies on biodiesel production from leather industry waste fat and its effect on diesel engine characteristics. Fuel, *276* (2020) 118000.
17. M. Sillanpää, A. Frey, R. Hillamo, A. S. Pennanen, R. O. Salonen, Organic, elemental and inorganic carbon in particulate matter of six urban environments in Europe. Atmos, Chem. Phys., **5**(11) (2005) 2869–2879.
18. I.V. Kothai, G.G. Saradhi, A. Pandit and V.D. Markwitz, Puranik. Chemical characterization and source identification of particulate matter at an urban site of Navi Mumbai, India, Aerosol Air Qual Res, *11* (2011) 560–569.
19. R. Rengarajan, A.K. Sudheer and M.M. Sarin, Aerosol acidity and secondary organic aerosol formation during wintertime over urban environment in western India. Atmos. Environ., *45* (2011) 1940–1945.
20. K. P. Shine, R. G. Derwent, D. J. Wuebbles, J. J. Morcrette, Radiative forcing of climate. Clim. change: The IPCC scientific assessment, (1990) 41–68.
21. S. Guo, M. Hu, Q. Guo, X. Zhang, M. Zheng, J. Zheng, C.C. Chang, J.J. Schauer and R. Zhang, Primary sources and secondary formation of organic aerosols in Beijing, China. Environ. Sci. Technol., *46* (2012) 9846–9853.
22. P.D. Safai, M.P. Raju, P.S.P. Rao and G. Pandithurai, Characterization of carbonaceous aerosols over the urban tropical location and a new approach to evaluate their climatic importance. Atmos. Environ., *92* (2014) 493–500.
23. W. Phairuang, P. Suwattiga, T. Chetiyanukornkul, S. Hongtieab, W. Limpaseni, F. Ikemori, M. Hata and M. Furuuchi, The influence of the open burning of agricultural biomass and forest

fires in Thailand on the carbonaceous components in size-fractionated particles. Environ. Pollut., *247* (2019) 238–247.
24. W. Phairuang, M. Inerb, M. Furuuchi, M. Hata, S. Tekasakul, P. Tekasakul, Size-fractionated carbonaceous aerosols down to PM0. 1 in southern Thailand: Local and long-range transport effects, Environ. Pollut., **260** (2020) 114031.
25. R. M. Flores, E. Mertoğlu, H. Özdemir, B. O. Akkoyunlu, G. Demir, A. Ünal, and M. Tayanç, A high-time resolution study of PM2. 5, organic carbon, and elemental carbon at an urban traffic site in Istanbul. Atmospheric Environment, **223** (2020) 117241.
26. D. Varrica, E. Tamburo, M. Vultaggio, I. Di Carlo, ATR–FTIR spectral analysis and soluble components of PM10 and PM2.5 particulate matter over the urban area of Palermo (Italy) during normal days and Saharan events, Int. J. Environ. Res., **16**(14) (2019).
27. I. Anıl, K. Golcuk, F. Karaca, ATR-FTIR spectroscopic study of functional groups in aerosols: The contribution of a Saharan dust transport to urban atmosphere in Istanbul, Turkey, Water, Air, Soil Pollut., **225**(3) (2014).
28. C. Coury and A.M. Dillner, A method to quantify organic functional groups and inorganic compounds in ambient aerosols using attenuated total reflectance FTIR spectroscopy and multivariate chemometric techniques. Atmos. Environ., *42* (2008) 5923–5932.
29. O.B. Popovicheva, E.D. Kireeva, N.K. Shonija and M. Vojtisek-lom, FTIR analysis of surface functionalities on particulate matter produced by off-road diesel engines operating on diesel and biofuel. Environ. Sci. Pollut. Res., *26* (2015) 4534–4544.
30. K.M. George, T.C. Ruthenburg, J. Smith, L. Yu, Q. Zhang, C. Anastasio and A.M. Dillner, FT-IR quantification of the carbonyl functional group in aqueous-phase secondary organic aerosol from phenols. Atmos. Environ., *100* (2015) 230–237.
31. S. Gilardoni, L.M. Russell, A. Sorooshian, R.C. Flagan, J.H. Seinfeld, T.S. Bates, P.K. Quinn, J.D. Allan, B. Williams, A.H. Goldstein, T.B. Onasch and D.R. Worsnop, Regional variation of organic functional groups in aerosol particles on four US east coast platforms during the International Consortium for Atmospheric Research on Transport and Transformation 2004 campaign, J. Geophys. Res. Atmos., **112**(D10) (2007).
32. C. Coury and A.M. Dillner, ATR-FTIR characterization of organic functional groups and inorganic ions in ambient aerosols at a rural site. Atmos. Environ., *43* (2009) 940–948.
33. A. Polidori, B. J. Turpin, C. I. Davidson, L. A. Rodenburg, F. Maimone, Organic PM 2.5: Fractionation by Polarity, FTIR Spectroscopy, and OM / OC Ratio for the Pittsburgh Aerosol, Aerosol Sci. Technol., **42**(3) (2008) 233–246.
34. I. L. Schneider, E. C. Teixeira, D. M. Agudelo-Castañeda, G. S. Silva, N. Balzaretti, M. F. Braga, L. F. S. Oliveira, FTIR analysis and evaluation of carcinogenic and mutagenic risks of nitro-polycyclic aromatic hydrocarbons in PM1. 0, Sci. Total Environ., **541** (2016) 1151–1160.
35. http://ddma.delhigovt.nic.in/wps/wcm/connect/doit_dm/DM/Home/COVID-19/Orders+of+DDMA+on+COVID+19/
36. https://app.cpcbccr.com / https://app.cpcbccr.com/ccr/#/caaqm-dashboard-all
37. R. Gadi, Shivani, S. K. Sharma, T. K. Mandal, Seasonal variation, source apportionment and source attributed health risk of fine carbonaceous aerosols over National Capital Region, India, Chemosphere, **237** (2019) 124500.
38. S. Gupta, R. Gadi, T.K. Mandal and S.K. Sharma, Seasonal variations and source profile of n-alkanes in particulate matter (PM10) at a heavy traffic site, Delhi. Environ. Monit. Assess., *189* (2017) 43.
39. S.K. Mishra, D. Khosla, M. Arora, C. Sharma, M.V.S.N. Prasad, S.G. Aggarwal, R.B. Gupta, S.R. Radhakrishnan, R. Guleria and R.K. Kotnala, SEM-EDS and FTIR characterization of aerosols during Diwali and Post Diwali festival over Delhi: implications to human health. J. Environ. Nanotechnol, *5* (2016) 12–26.
40. V. Goel, S.K. Mishra, C. Sharma, B. Sarangi, S.G. Aggarwal, R. Agnihotri, R.K. Kotnala, A non-destructive FTIR method for the determination of ammonium and sulfate in urban PM2.5 samples. MAPAN-J. Metrol. Soc India, **33**(3) (2018) 209–215.
41. Census 2011 and‘ Economic Survey of Delhi, 2018–19 [http://delhiplanning.nic.in/sites/default/files/2%29%20Demographic%20Profile.pdf]
42. T. Saud, R. Gautam, T. K. Mandal, Ranu Gadi, D. P. Singh, S. K. Sharma, Manisha Dahiya, and M. Saxena. “Emission estimates of organic and elemental carbon from household biomass fuel used over the Indo-Gangetic Plain (IGP), India, Atmos. Environ. **61** (2012) 212–220.
43. T. Saud, M. Saxena, D.P. Singh, M. Dahiya, S.K. Sharma, A. Datta, R. Gadi and T.K. Mandal, Spatial variation of chemical constituents from the burning of commonly used biomass fuels in rural areas of the Indo-Gangetic Plain (IGP), India. Atmos. Environ., *71* (2013) 158–169.
44. S. K. Sharma, T. K. Mandal, M. Saxena, A. Sharma, A. Datta, T. Saud, Variation of OC, EC, WSIC and trace metals of PM10 in Delhi, India, J. Atmos. Sol.-Terr. Phys, **113** (2014) 10–22.
45. S. Gupta and R. Gadi, Temporal Variation of Phthalic Acid Esters (PAEs) in Ambient Atmosphere of Delhi. Bull. Environ. Contam. Toxicol., *101* (2018) 153–159.
46. R. Shivani, S.K. Gadi, T.K. Sharma, R. Mandal, S. Kumar, S. Mona and S. Kumar, Kumar, Levels and sources of organic compounds in fine ambient aerosols over National Capital Region of India. Environ. Sci. Pollut. Res., *25* (2018) 31071–31090.
47. R. Banoo, S. K. Sharma, T. K. Mandal, Seasonal characteristics and sources of carbonaceous components and elements of PM10 (2010–2019) in Delhi, India, J. Atmos. Chem, (2021) 1–20.
48. P. Pant, A. Shukla, S. D. Kohl, J. C. Chow, J. G. Watson, R. M. Harrison, Characterization of ambient PM2. 5 at a pollution hotspot in New Delhi, India and inference of sources, Atmos. Environ., **109** (2015)178–189.
49. C. Radulescu, C. Stihi, S. Iordache, D. Dunea, I. D. Dulama, Characterization of urban atmospheric PM2. 5 by ATR-FTIR, ICP-MS and SEM-EDS techniques, Rev. Chim, **68** (2017) 805–810.
50. T. Siciliano, M. Siciliano, C. Malitesta, A. Proto, R. Cucciniello, A. Giove, A., S. Iacobellis, A. Genga, Carbonaceous PM10 and PM2.5 and secondary organic aerosol in a coastal rural site near Brindisi (Southern Italy), Environ. Sci. Pollut. Res., **25**(24) (2018) 23929–23945.
51. P. Rajput and M.M. Sarin, Polar and non-polar organic aerosols from large-scale agricultural-waste burning emissions in Northern India: implications to organic mass-to-organic carbon ratio. Chemosphere, *103* (2014) 74–79.
52. Y. Han, Y. Chen, S. Ahmad, Y. Feng, F. Zhang, W. Song, F. Cao, Y. Zhang, X. Yang, J. Li and G. Zhang, High time-and size-resolved measurements of PM and chemical composition from coal combustion: implications for the EC formation process. Environ. Sci. Tech., *52* (2018) 6676–6685.
53. A. Kumar, S. Singh, N. Kumar, N. Singh, K. Kumar and S. Chourasiya, Assessment of carbonaceous fractions in ambient aerosols at high altitude and lowland urban locations of Kumaon Province, Indian Himalaya. SN Applied Sciences, *3* (2021) 1–14.
54. H.S. El-Zanan, D.H. Lowenthal, B. Zielinska, J.C. Chow and N. Kumar, Determination of the organic aerosol mass to organic carbon ratio in IMPROVE samples. Chemosphere, *60* (2005) 485–496.
55. S. Jain, S. K. Sharma, N. Vijayan, and T. K. Mandal, Seasonal characteristics of aerosols (PM2. 5 and PM10) and their source apportionment using PMF: a four year study over Delhi, India. Environmental Pollution, **262** (2020) 114337.

56. S.M. Fulk and G.T. Rochelle, Quantification of gas and aerosol-phase piperazine emissions by FTIR under variable bench-scale absorber conditions. Energy Procedia, *63* (2014) 871–883.
57. Xu, J., Hu, W., Liang, D., & Gao, P. (2020). Photochemical impacts on the toxicity of PM2.5, Crit. Rev. Environ. Sci. Technol., 1–27.
58. L. Xing, T.M. Fu, J.J. Cao, S.C. Lee, G.H. Wang, K.F. Ho, M.C. Cheng, C.F. You and T.J. Wang, Seasonal and spatial variability of the OM/OC mass ratios and high regional correlation between oxalic acid and zinc in Chinese urban organic aerosols. Atmos. Chem. Phys., *13* (2013) 4307–4318.
59. S.G. Brown, T. Lee, P.T. Roberts and J.L. Collett Jr., Variations in the OM/OC ratio of urban organic aerosol next to a major roadway. Journal of the Air & Waste Management Association, *63* (2013) 1422–1433.
60. Y.C. Chien, M. Lu, M. Chai and F.J. Boreo, Characterization of biodiesel and biodiesel particulate matter by TG, TG− MS, and FTIR. Energy Fuels, *23* (2009) 202–206.
61. J. Coates, Interpretation of infrared spectra, a practical approach, in Encyclopedia of Analytical Chemistry, R.A. Meyers (Ed.), John Wiley & Sons Ltd, Chichester, 2000.
62. D. Liu, T. Lin, J. H. Syed, Z. Cheng, Y. Xu, K. Li, G. Zhang, J. Li, J., Concentration, source identification, and exposure risk assessment of PM2. 5-bound parent PAHs and nitro-PAHs in atmosphere from typical Chinese cities, Scientific Reports, **7**(1), (2017) 1–12.
63. S. Tomaz, J.L. Jaffrezo, O. Favez, E. Perraudin, E. Villenave and A. Albinet, Sources and atmospheric chemistry of oxy-and nitro-PAHs in the ambient air of Grenoble (France). Atmos. Environ., *161* (2017) 144–154.
64. Z. Ji, R. Dai and Z. Zhang, Characterization of fine particulate matter in ambient air by combining TEM and multiple spectroscopic techniques–NMR, FTIR and Raman spectroscopy. Environ. Sci. Process Impacts, *17* (2015) 552–560.
65. Y. Ulusoy, Investigation of particulate matter by FTIR, TEM and elemental analyses in a diesel engine operating on diesel and waste cooking oil-biodiesel. Environ. Sci. Pollut. Res., *27* (2019) 500–509.
66. P.M. Fine, C. Sioutas and P.A. Solomon, Secondary particulate matter in the United states: Insights from the Particulate Matter Supersites Program and Related Studies. J. Air Waste Manage. Assoc., *58* (2008) 234–253.
67. R. Ravisankar, S. Kiruba, P. Eswaran, G. Senthilkumar and A. Chandrasekaran, Mineralogical characterization studies of ancient potteries of Tamilnadu. India by FT-IR spectroscopic technique, E-J Chem., *7* (2010) S185–S190.
68. J. Simao, E. Ruiz-agudo and C. Rodriguez-navarro, Effects of particulate matter from gasoline and diesel vehicle exhaust emissions on silicate stones sulfation. Atmos. Environ., *40* (2006) 6905–6917.
69. L. Medeghini, S. Mignardi, C. De Vito and A. Maria, Evaluation of a FTIR data pretreatment method for Principal Component Analysis applied to archaeological ceramics. Microchem. J., *125* (2016) 224–229.
70. M. Tang, J. M. Alexander, D. Kwon, A. D. Estillore, O. Laskina, M. A. Young, D. Kleiber Paul, H. Vicki and V. H. Grassian, Optical and physicochemical properties of brown carbon aerosol: Light scattering, FTIR extinction spectroscopy, and hygroscopic growth, J. Phys. Chem. A, **120**(24) (2016) 4155–4166).